Using quantum annealers to calculate ground state properties of molecules

Justin Copenhaver, Adam Wasserman, and Birgit Wehefritz-Kaufmann

View Online   Export Citation   CrossMark

ARTICLES YOU MAY BE INTERESTED IN

AIP
Publishing

Using quantum annealers to calculate ground state properties of molecules

View Online   Export Citation   CrossMark

Justin Copenhaver,[1,a] (ID)   Adam Wasserman,[1,2,3] (ID)   and Birgit Wehefritz-Kaufmann[1,3,4] (ID)

AFFILIATIONS

[1] Department of Physics and Astronomy, Purdue University, West Lafayette, Indiana 47907, USA
[2] Department of Chemistry, Purdue University, West Lafayette, Indiana 47907, USA
[3] Purdue Quantum Science and Engineering Institute, Purdue University, West Lafayette, Indiana 47907, USA
[4] Department of Mathematics, Purdue University, West Lafayette, Indiana 47907, USA

[a] Author to whom correspondence should be addressed: jcopenh@purdue.edu

ABSTRACT

Quantum annealers are an alternative approach to quantum computing, which make use of the adiabatic theorem to efficiently find the ground state of a physically realizable Hamiltonian. Such devices are currently commercially available and have been successfully applied to several combinatorial and discrete optimization problems. However, the application of quantum annealers to problems in chemistry remains a relatively sparse area of research due to the difficulty in mapping molecular systems to the Ising model Hamiltonian. In this paper, we review two different methods for finding the ground state of molecular Hamiltonians using Ising model-based quantum annealers. In addition, we compare the relative effectiveness of each method by calculating the binding energies, bond lengths, and bond angles of the H_3^+ and H_2O molecules and mapping their potential energy curves. We also assess the resource requirements of each method by determining the number of qubits and computation time required to simulate each molecule using various parameter values. While each of these methods is capable of accurately predicting the ground state properties of small molecules, we find that they are still outperformed by modern classical algorithms and that the scaling of the resource requirements remains a challenge.

Published under license by AIP Publishing. https://doi.org/10.1063/5.0030397

I. INTRODUCTION

The application of quantum computers to quantum chemistry has the potential to enable the simulation of large molecular systems that would otherwise be unattainable on classical computers. Thus far, several algorithms have been devised to simulate molecular systems on gate-based quantum computers, including the quantum phase estimation (QPE) and variational quantum eigensolver (VQE) algorithms,[1,2] as well as various quantum machine learning algorithms.[3,4] While such algorithms are promising, the difficulty of constructing gate-based quantum computers has meant that their applications to quantum chemistry have been limited. Interest in quantum annealers as potential alternatives to gate-based quantum computers has increased recently, with new methods being proposed to map quantum chemistry problems onto quantum annealers.[5,6] Here, we review some of the basics of quantum annealing and how it

can be applied to the electronic structure problem, give a detailed explanation and comparison of the recently developed mappings, and use these methods to calculate the ground state properties of the H_3^+ and H_2O molecules. In addition, we have open-sourced our code at https://github.com/jcopenh/Quantum-Chemistry-with-Annealers so that others can see how the techniques discussed might be implemented.

Quantum annealing is an optimization metaheuristic that exploits quantum tunneling effects to efficiently find the minimum of an objective function.[7–9] The governing principle of quantum annealers is the adiabatic theorem, which states that if a system is in an eigenstate of a governing Hamiltonian, which is slowly perturbed, then the system will remain in the instantaneous eigenstate of the perturbed Hamiltonian so long as the rate of change is slow enough and there is an energy gap between nearby eigenstates.[10] The annealer begins in the ground state of some easy-to-prepare initial

Hamiltonian H_I and is then allowed to evolve approximately adiabatically, while the governing Hamiltonian $H(t)$ is slowly perturbed to a final Hamiltonian H_F according to

$$H(t) = A(t)H_I + B(t)H_F, \tag{1}$$

where the functions $A(t)$ and $B(t)$ are collectively referred to as the annealing schedule and satisfy the constraints $A(0) \gg B(0) \approx 0$ and $B(T) \gg A(T) \approx 0$, where T is the total annealing time.[7,11,35] At the end of the annealing process, $H(T) = H_F$ and the current state of the annealer is taken to be the ground state of H_F. Thus, by encoding information about a problem into the previously unknown ground state of H_F, the annealer "solves" the problem by taking advantage of the adiabatic theorem to search for the ground state.

The prototypical example of a governing Hamiltonian is the transverse-field Ising model,[7]

$$H(t) = A(t)\sum_i \sigma_x^i + B(t)\left[\sum_i h_i \sigma_z^i + \sum_{i<j} J_{ij}\sigma_z^i \sigma_z^j\right], \tag{2}$$

where h_i are the qubit biases, J_{ij} are the coupling coefficients, and σ_α^i are Pauli operators acting on the ith qubit of the annealer. The transverse-field term is used as the initial Hamiltonian H_I, leaving the remaining terms, which form a regular Ising spin-glass model, as the final Hamiltonian,

$$H_F = \sum_i h_i \sigma_z^i + \sum_{i<j} J_{ij}\sigma_z^i \sigma_z^j. \tag{3}$$

The transverse-field Ising model is stoquastic, meaning that all off-diagonal terms are real and non-positive. This is of great consequence for the capabilities of Ising model-based annealers, as any adiabatic quantum computer must implement a non-stoquastic Hamiltonian to be universal.[12–14] Indeed, previous experiments have shown annealers based on stoquastic Hamiltonians to be of limited applicability,[11,15] leading to the development of several non-stoquastic annealer designs.[13,16,17] However, given that such implementations are very much still in development, we will focus on the application of Ising model-based annealers in this paper.

The main challenge with utilizing Ising model-based quantum annealers to solve quantum chemistry problems lies in the difficulty of finding H_F, as given in Eq. (3). In Sec. II, we give an overview of how the electronic structure problem can be mapped to an Ising model Hamiltonian.

II. MAPPING MOLECULAR HAMILTONIANS TO THE ISING MODEL

The electronic structure of a molecule describes the motions and spin properties of electrons within the molecule. Descriptions of the electronic structure are typically given as solutions to the Schrödinger equation after applying the Born–Oppenheimer approximation, which assumes the nuclei to be fixed in space relative to the center of the molecule. The first-quantized Hamiltonian in atomic units is given by

$$H = -\sum_i \frac{\nabla_i^2}{2} - \sum_A \frac{\nabla_A^2}{2M_A} - \sum_{i,A} \frac{Z_A}{|\boldsymbol{r}_i - \boldsymbol{R}_A|} + \sum_{i<j} \frac{1}{|\boldsymbol{r}_i - \boldsymbol{r}_j|} + \sum_{A<B} \frac{Z_A Z_B}{|\boldsymbol{R}_A - \boldsymbol{R}_B|}, \tag{4}$$

where $\boldsymbol{r}_i$ is the position of electron i and $\boldsymbol{R}_A$, M_A, and Z_A are the position, mass, and charge of nuclei A.

Using the second quantization formalism, one can write H in terms of fermionic creation and annihilation operators $a_i^\dagger$ and a_i by choosing a basis set, calculating the one-body and two-body integrals h_{ij} and h_{ijkl}, and constructing H as

$$H = \sum_{i,j} h_{ij} a_i^\dagger a_j + \frac{1}{2}\sum_{i,j,k,l} h_{ijkl} a_i^\dagger a_j^\dagger a_k a_l. \tag{5}$$

Eigenstates of the Hamiltonian are now given by linear combinations of the occupation-number representation,

$$|\Psi\rangle = |n_1, n_2, \ldots, n_M\rangle, \tag{6}$$

with M being the total number of spin orbitals in the chosen basis set and $n_i \in \{0, 1\}$ representing whether or not spin orbital i is filled by an electron. The state $|\Psi\rangle$ is equivalent to the Slater determinant formed using the filled spin orbitals. In addition, one can restrict the active space of the molecule to a subset of the spin orbitals, reducing the number of fermionic operators in H at the cost of potentially missing lower energy solutions. In this case, M is now the number of spin orbitals in the chosen active space.

Note that the second quantization formalism does not conserve the particle number, i.e., the eigenstates of H in Eq. (5) are in the form of Eq. (6) with anywhere from 0 to M electrons filling the spin orbitals. In many cases, however, one is only interested in solutions with a fixed number of electrons N. In order to ensure that the ground state solution for H has N electrons, one can construct the total number operator

$$\hat{N} = \sum_{i=1}^{M} a_i^\dagger a_i \tag{7}$$

and use it to add a penalty term to H,

$$H' = H + w(N - \hat{N})^2, \tag{8}$$

where w is a weight factor large enough to ensure that the eigenvalues corresponding to solutions with N electrons are less than all other eigenvalues.[18] One can similarly add penalty terms to H to fix the total spin of the system, or any other quantum observable, so long as one can readily construct the corresponding operator in terms of the creation and annihilation operators.

After writing H in terms of creation and annihilation operators, one must transform H into a sum of Pauli words,

$$H = \sum_i \alpha_i P_i, \tag{9}$$

with the Pauli word P_i being of the form

$$P_i = \pm\{I, \sigma_x, \sigma_y, \sigma_z\}^{\otimes m}, \tag{10}$$

where $m \le M$ is the number of qubits. Here, H acts on the m-qubit space spanned by basis states of the form

$$|\phi\rangle = \prod_{i=1}^{m} |z_i\rangle = |z_1, z_2, \ldots, z_m\rangle \tag{11}$$

such that $z_i \in \{0, 1\}$ is equal to 0 if qubit i is in the spin-up state and 1 if it is in the spin-down state. Any state $|\Psi\rangle$ in this m-qubit space can then be written as a sum of these 2^m basis states,

$$|\Psi\rangle = \sum_{i=1}^{2^m} a_i |\phi_i\rangle. \tag{12}$$

Several transformations exist to transform H into the form of Eq. (9), including the Jordan–Wigner (JW) transformation, the Bravyi–Kitaev (BK) transformation, and the parity encoding.[19–21] Once this is done, it is often helpful to reduce the number of qubits required to simulate the molecule by exploiting its symmetries and conservation properties. A detailed explanation of this procedure can be found in Ref. 22 along with insight into how such reductions can be found using the knowledge of the molecule's point group symmetries in Ref. 23.

The next step in transforming H into the form of Eq. (3) is perhaps the most difficult. We are aware of two methods for mapping Eq. (9) onto the Ising model Hamiltonian: the Xia–Bian–Kais (XBK) transformation proposed in Ref. 5 and the Bloch angle mapping used in Ref. 6. These methods will be described in detail in Secs. III and IV. Both will result in a diagonal Hamiltonian in the form of a k-local sum of z-type Pauli operators,

$$H = \sum_i \alpha_i \sigma_z^i + \sum_{i<j} \alpha_{ij} \sigma_z^i \sigma_z^j + \sum_{i<j<k} \alpha_{ijk} \sigma_z^i \sigma_z^j \sigma_z^k + \cdots, \tag{13}$$

which now acts on the mapped m'-qubit space where $m' \ge m$.

The k-local Hamiltonian of Eq. (13) must then be reduced to a two-local Hamiltonian with the same ground state. This process, known as quadratization, in general, leads to the introduction of several auxiliary qubits, which account for the missing higher order terms.[24,25] After quadratization, H should now be in the form of Eq. (3) and can be embedded on the quantum annealer to find the ground state.

III. XIA–BIAN–KAIS METHOD

The XBK transformation maps states from the m-qubit space associated with Eq. (9) to an rm-qubit space, where r is a variational parameter that represents the number of copies of the original m qubits.[5] Each Pauli operator in this new space can be represented using tensor products of the identity and z-type Pauli operators. By increasing r, one expands the space in which the quantum annealer searches for the ground state, thus increasing the accuracy of the energy calculations.

The mapping of each Pauli operator to the new space is given by

$$\sigma_x^i \to \frac{1 - \sigma_z^{i_j}\sigma_z^{i_k}}{2}, \quad \sigma_y^i \to i\frac{\sigma_z^{i_k} - \sigma_z^{i_j}}{2},$$
$$\sigma_z^i \to \frac{\sigma_z^{i_j} + \sigma_z^{i_k}}{2}, \quad I^i \to \frac{1 + \sigma_z^{i_j}\sigma_z^{i_k}}{2}, \tag{14}$$

with $\sigma_z^{i_j}$ being the z-type Pauli operator acting on ith qubit of the jth m-qubit subspace. For a given i and j, applying Eq. (14) to each operator in Eq. (9) will map H to a "sub-Hamiltonian" $H^{(i,j)}$ acting on a $2m$-qubit space. In order to properly account for each of the $\lceil \frac{r}{2} \rceil$ possible sign combinations of the sub-Hamiltonians, one defines a sign parameter $0 \le p \le \lfloor \frac{r}{2} \rfloor$ and constructs the sign function

$$S_p(i) = \begin{cases} -1, & i \le p, \\ 1, & \text{else.} \end{cases} \tag{15}$$

The $\lceil \frac{r}{2} \rceil$ possible rm-qubit Hamiltonians are obtained by summing over $H^{(i,j)}$ for each combination of $1 \le i, j \le r$ and taking into account the signs associated with each sub-Hamiltonian,

$$H_p' = \sum_{i,j \le r} H^{(i,j)} S_p(i) S_p(j). \tag{16}$$

Each of the H_p' will explore a sector of the rm-qubit space.

It can be shown that if the eigenvalue of the original H corresponding to the m-qubit state $|\Psi\rangle$ is λ', then the eigenvalue of H_p' corresponding to the rm-qubit state $|\psi'\rangle$ is $\lambda' \sum_i b_i^2$, where b_i is the number of times the basis state $|\phi_i\rangle$ appears in $|\psi'\rangle$.[5] Thus, one can construct an operator C_p that keeps track of $\sum_i b_i^2$,

$$C_p = \sum_{\pm} \left[\sum_{i=1}^r \left(S_p(i) \prod_{k=1_i}^{m_i} \frac{1 \pm \sigma_z^k}{2} \right) \right]^2, \tag{17}$$

where $\sum_{\pm}$ means to sum over all combinations of the plus–minus signs. Given H_p' and C_p, the procedure to find the minimum eigenvalue of H for the pth sector is as follows: we choose a starting value λ and construct the operator $D_{p,\lambda} = H_p' - \lambda C_p$, whose minimum eigenvalue is $\sum_i b_i^2 (\lambda' - \lambda)$ so long as it is less than 0. After quadratizating this operator, we can map it to the quantum annealer by taking $H_F = D_{p,\lambda}$ to find $\sum_i b_i^2 (\lambda' - \lambda)$. Evaluating C_p at the ground state, we obtain $\sum_i b_i^2$, which allows us to solve for λ'. Setting $\lambda = \lambda'$, we repeat this process until the minimum eigenvalue of $D_{p,\lambda}$ is greater than or equal to 0. The minimum eigenvalue is then taken as λ' when this process terminates.

By searching through all values of p, we find the minimum eigenvalue of H for those states mapped to the rm-qubit space. To retrieve the m-qubit state $|\Psi\rangle$ from the rm-qubit state $|\psi'\rangle$, we use the fact that for large enough r, the coefficient a_i for the basis state $|\phi_i\rangle$ can be approximated by

$$a_i \approx \frac{b_i S(b_i)}{\sqrt{\sum_j b_j^2}}, \tag{18}$$

where by $S(b_i)$ we mean the sign of the sum of $S_p(i)$ for all m-qubit spaces that are in the ith basis state using the value of p

corresponding to the sector in which the ground state was found. We then use Eq. (12) to obtain $|\Psi\rangle$.

Beyond the pre-processing required to construct and quadratize $D_{p,\lambda}$, the optimization in the XBK method is performed solely on the quantum annealer. However, this pre-processing becomes quite expensive for larger values of m and r. The number of qubits in $D_{p,\lambda}$ before quadratization is rm, and due to the large number of auxiliary qubits introduced during the quadratization procedure, the final number of qubits required to simulate $D_{p,\lambda}$ on the quantum annealer can quickly surpass what is available on modern systems. Thus, the application of the XBK method to the accurate simulation of larger molecular systems is currently impractical.

IV. QUBIT COUPLED CLUSTER METHOD

The qubit coupled cluster (QCC) method is a hybrid classical–quantum method that utilizes the quantum annealer to improve the convergence rate of a classical optimization routine.[6,26] The QCC method begins with the qubit mean-field (QMF) description, which assumes that the ground state of H is of the form

$$|\Psi\rangle = \prod_{i=1}^{m} |\Omega_i\rangle \qquad (19)$$

such that $|\Omega_i\rangle$ is the spin-coherent state of the ith qubit,

$$|\Omega_i\rangle = \cos\left(\frac{\theta_i}{2}\right)|0\rangle + e^{i\varphi_i}\sin\left(\frac{\theta_i}{2}\right)|1\rangle, \qquad (20)$$

where $\varphi_i \in [0, 2\pi)$ and $\theta_i \in [0, \pi)$ are the azimuthal and polar angles of the Bloch sphere, respectively. The set of all φ_i and θ_i are collectively called the Bloch angles of $|\Psi\rangle$. The QMF energy is then defined as the expectation value of H evaluated at $|\Psi\rangle$ for optimized Bloch angles.

The Hamiltonian in Eq. (9) can be converted into a real-valued function whose global minimum is equal to the QMF energy by mapping the Pauli operators to the Bloch angles,

$$\begin{aligned}
\sigma_x^i &\to \cos\varphi_i \sin\theta_i, \\
\sigma_y^i &\to \sin\varphi_i \sin\theta_i, \\
\sigma_z^i &\to \cos\theta_i.
\end{aligned} \qquad (21)$$

With H now in the form of a continuous optimization problem, a classical optimization routine can be used to find the QMF energy. Using the optimal Bloch angles, one can then use Eq. (20) to reconstruct the state corresponding to the QMF energy.

The next step of the QCC method is to introduce a multiqubit unitary transformation to "entangle" the qubits and simulate electron-correlation effects. The QCC transformation is given by

$$U(\boldsymbol{\tau}) = \prod_{k=1}^{N_{ent}} \exp(-i\tau_k P_k/2), \qquad (22)$$

where P_k is a multi-qubit Pauli word called an entangler, $\tau_k \in [0, 2\pi)$ is the corresponding entangler amplitude, and N_{ent} is the total number of entanglers used. As N_{ent} is increased, more electron-correlation effects are taken into account, improving the accuracy of the method. In addition, some entanglers will be more important in the simulation than others, necessitating a procedure to find the optimal entanglers for the system at hand as in Ref. 26. The transformed Hamiltonian H' can easily be found using the recursive formula

$$H^{(k)}(\boldsymbol{\tau}) = H^{(k-1)} - i\frac{\sin\tau_k}{2}[H^{(k-1)}, P_k] + \frac{1}{2}(1-\cos\tau_k)P_k[H^{(k-1)}, P_k] \qquad (23)$$

for $1 \le k \le N_{ent}$, where $H^{(0)} = H$ and $H^{(N_{ent})} = U^\dagger H U = H'$. The QCC energy is defined as the expectation value of H' for optimized Bloch angles and entangler amplitudes. Using the Bloch angle mapping given by Eq. (21), H' can be converted into a continuous optimization problem over the set of Bloch angles and entangler amplitudes, where the global minimum is now the QCC energy.

The quantum annealer is brought into the QCC method by recognizing the symmetries of the trigonometric functions present in H. The even–odd nature of these functions allows for their domains to be "folded" along their axis of symmetry by introducing discrete variables $Z_i \in \{-1, 1\}$. These foldings turn H into a mixed discrete-continuous optimization problem, which is solved in a step-based fashion. For fixed values of the continuous variables, H will be in the form of Eq. (13) and, after quadratization, can be mapped to the annealer as $H_F = H$. After using the annealer to optimize the discrete part, the classical computer is used to perform the continuous optimization with the discrete variables fixed.

By introducing the foldings, the chances of finding the QMF and QCC energies can be greatly improved at the cost of the discrete optimization step performed by the annealer. The foldings, which can be found in more detail in Ref. 6, allow for one folding in the θ_i variables, two foldings in the φ_i variables, and two foldings in the τ_k variables. Thus, there are up to $3m$ discrete variables to be optimized when finding the QMF energy and up to $3m + 2N_{ent}$ discrete variables when finding the QCC energy. The number of qubits before quadratization is then equal to the number of discrete variables being optimized.

Unlike the the XBK method, the QCC method relies on a classical computer to perform the bulk of the optimization; the quantum annealer simply increases the chances of finding the correct minimal energy. Due to this reliance, the potential for a substantial improvement over other classical algorithms is dubious. However, with the correct choice of entanglers and foldings, the QCC method can produce results comparable to the XBK method while using fewer qubits on the annealer.

V. RESULTS

In order to compare the relative accuracy of the XBK and QCC methods, we have used each method to calculate the binding energy and bond length of H_3^+ and the binding energy, bond length, and bond angle of H_2O. The bond length and bond angles are taken to be those that minimize the ground state energy, and

the binding energies are calculated by taking the difference between the ground state energy calculated at the disassociation limit (>10 Å) and the minimum energy. We have also used each method to produce the potential energy curves of each molecule. To be consistent, we use the same number of qubits before quadratization for both methods. We compare the results that we obtained to those of the restricted Hartree–Fock (RHF) and complete active space configuration interaction (CASCI) methods.[27] Note that the CASCI method is exact for the chosen basis set and active space, and it is equivalent to the full configuration interaction (FCI) method when the active space includes all spin orbitals. We therefore use the CASCI method to measure the accuracy of the XBK and QCC methods.

The scalability of the XBK and QCC methods depends on the number of post-quadratization qubits needed to run the methods and the total computation time. The largest quantum annealer currently available is D-Wave's new Advantage system, which has over 5000 qubits with 15-qubit connectivity. To compare the computational costs of each method, we plot how the number of post-quadratization qubits scales with the number of pre-quadratization qubits and thus with the parameters of each method. We also plot the time required to compute a single ground state energy vs the number of pre-quadratization qubits to gauge how the computation time scales with the size and accuracy of the calculations.

For all calculations, we utilize the PySCF and OpenFermion modules to construct the relevant operators and to calculate the RHF and CASCI energies.[28,29] The total number operator is used to fix the number of electrons as in Eq. (8), and the Bravyi–Kitaev transformation is used to map the fermionic Hamiltonian to Pauli operators. We use D-Wave's Ocean Software to quadratize the Hamiltonians and embed them on the annealer.[30,31] D-Wave's Advantage quantum annealer is used for the time-sensitive calculations; however, due to the limited computational time available on the D-Wave, we use the simulated annealer available through the Ocean Software for the remaining calculations. All classical computations are done on an AMD Ryzen 7 1700X eight-core processor running at 3400 MHz. We use the L-BFGS-B algorithm to perform the continuous optimization in the QCC method.[32] The code we used for this project can be found at https://github.com/jcopenh/Quantum-Chemistry-with-Annealers.

A. Trihydrogen cation

As the most common ion in the universe, H_3^+ provides an interesting subject to test the efficacy of the XBK and QCC methods for ions. The nuclei of H_3^+ form an equilateral triangle with an H–H equilibrium bond length of about 0.9 Å. As far as we are aware, this is the first time H_3^+ will be modeled on a quantum annealer. For H_3^+, we use the STO-6G basis set with all six spin-orbitals, and the Hamiltonian is written using four qubits after applying symmetry reductions. We were able to run the XBK method with up to $r = 4$, necessitating 16 pre-quadratization qubits. For the QCC method, we set $N_{ent} = 4$ and folded the θ_i and φ_i variables once and the τ_k variables twice, again needing 16 qubits.

The potential energy curve associated with symmetrically stretching the H–H bonds is shown in Fig. 1. Here, the CASCI energies are exact for the STO-6G basis since all spin orbitals are included
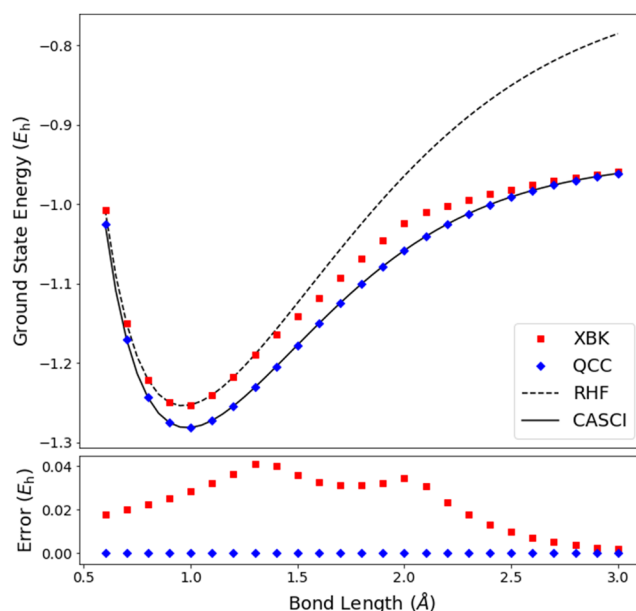

FIG. 1. Potential energy curve for H_3^+ created by symmetrically varying the H–H bond lengths. The difference between the XBK and QCC energies and those calculated using the CASCI method is plotted below.

in the active space. At $r = 4$, the XBK method is able to find energies lower than the RHF energies except near the equilibrium length but is outperformed by the QCC method, which consistently finds the ground state energies to within chemical accuracy (<0.002 Hartree). Table I shows the values for the binding energy and bond length of H_3^+ calculated using the various methods. The XBK method shows improvement over the RHF method, while the QCC method gives the exact values.

In Fig. 2, we plot the qubit scaling for the H_3^+ molecule at a bond length of 1.2 Å. For the XBK method, the value of r is varied, while for the QCC method, we vary N_{ent} and fold all three variables once. Note that for H_3^+ with the chosen settings, the number of pre-quadratization qubits will go as $4r$ for the XBK method and $8 + N_{ent}$ for the QCC method. Figure 3 shows the time scaling of the H_3^+ molecule at 1.2 Å. The computation time averaged over five runs is broken into two components. The "classical" time includes the time required to convert the electronic Hamiltonian to Pauli operators and find an embedding for the Ising model and any

TABLE I. Binding energy and bond length of H_3^+ calculated using various methods.

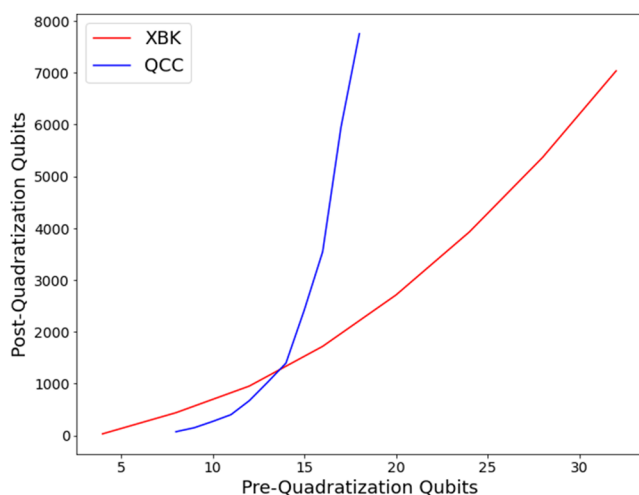| Method	BE (E_h)	BL (Å)
XBK	0.312	0.965
QCC	0.339	0.984
RHF	0.560	0.965
CASCI	0.339	0.984

FIG. 2. Number of post-quadratization qubits required to run each method vs the number of pre-quadratization qubits for H_3^+ with a bond length of 1.2 Å.

other procedure performed on the classical processor. The "annealing" time is the total amount of time the quantum annealer spends on the calculation, which includes the physical annealing as well as several other steps, as reported by D-Wave's qpu_access_time variable. For reference, the convergence time of the CASCI method was 0.23 s.

As demonstrated in Figs. 2 and 3, the resource requirements of the XBK and QCC methods do not scale well with the parameters of each method. The number of post-quadratization qubits required to simulate H_3^+ surpasses what is available on D-Wave's Advantage system after $r = 6$ for the XBK method and $N_{ent} = 8$ for the QCC method. Similarly, the computation time of each method
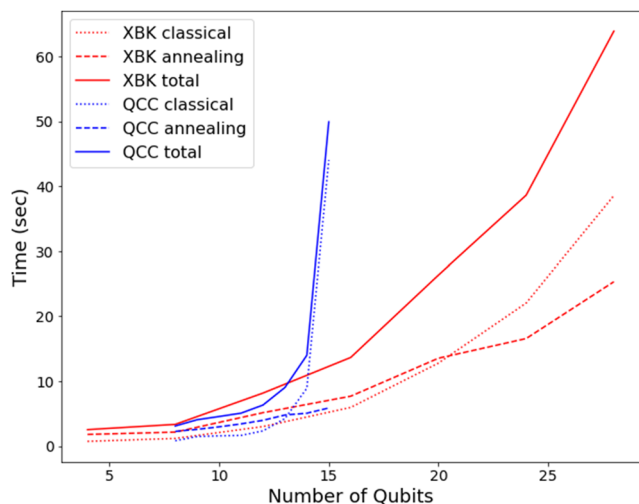

FIG. 3. Breakdown of the computation times of the XBK and QCC methods vs the number of pre-quadratization qubits for H_3^+ with a bond length of 1.2 Å.
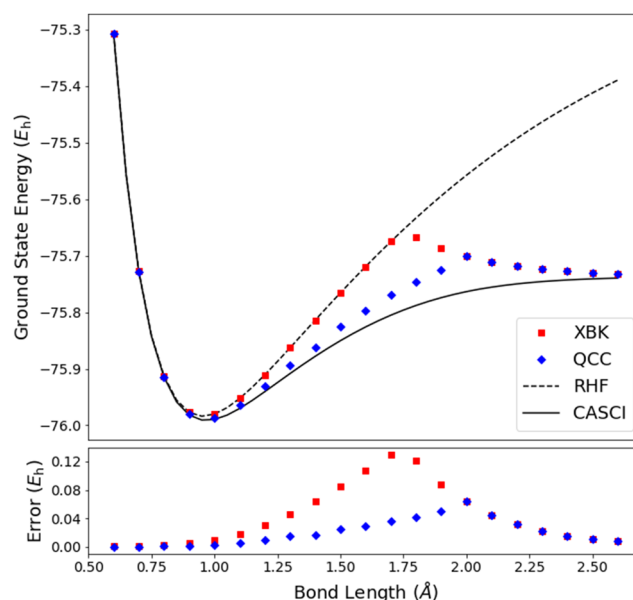

FIG. 4. Potential energy curve for H_2O created by symmetrically varying the O–H bond lengths with a fixed bond angle of 104.48°. The difference between the XBK and QCC energies and those calculated using the CASCI method is plotted below.

increases exponentially with the number of qubits. Since more qubits are required to accurately calculate the energies of larger molecular systems, this result indicates that neither method will scale well with the system size.
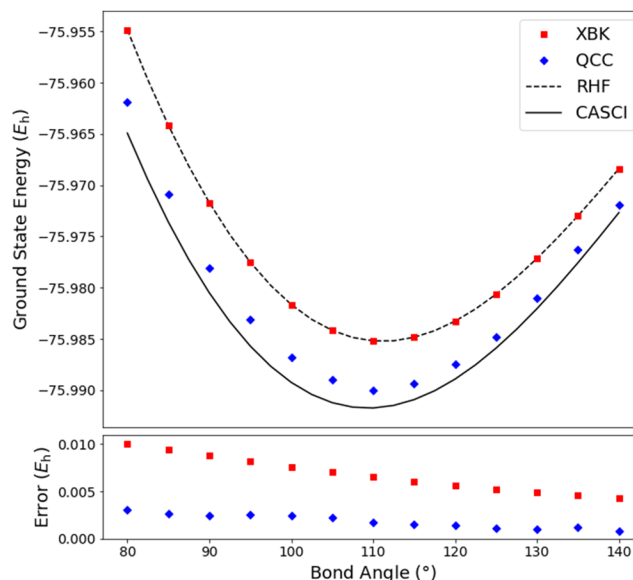

FIG. 5. Potential energy curve for H_2O created by varying the angle between the O–H bonds with fixed bond lengths of 0.9578 Å. The difference between the XBK and QCC energies and those calculated using the CASCI method is plotted below.
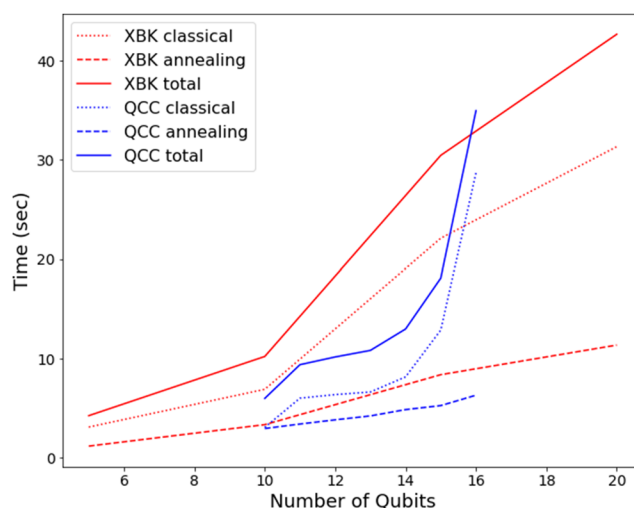
TABLE II. Binding energy, bond length, and bond angle of H_2O calculated using various methods.

Method	BE (E_h)	BL (Å)	BA (deg)
XBK	0.257	0.954	111.2
QCC	0.262	0.960	110.5
RHF	0.602	0.954	111.2
CASCI	0.265	0.968	109.4

B. Water molecule

The water molecule is a slightly larger molecule than H_3^+ and thus provides a better test for the limits of the XBK and QCC methods. We use the 6-31G basis set to construct the fermionic Hamiltonian but restrict the active space to just eight spin-orbitals and four electrons due to computational constraints. Since the active space does not include all the spin orbitals, the CASCI method is not exact. After applying symmetry reductions, the Hamiltonian can be written using five qubits. The XBK method was only run with $r = 2$, while for the QCC method, $N_{ent} = 5$ and the θ_i and τ_k variables were folded once; thus, both methods used ten pre-quadratization qubits.

Figure 4 shows the potential energy curve created by symmetrically stretching the O–H bonds, keeping the bond angle constant at $104.48°$. At $r = 2$, the XBK method follows the RHF curve near the equilibrium point but then quickly converges to the CASCI curve. The QCC method, meanwhile, consistently finds energies below the RHF curve, with the most accurate results again found near the equilibrium point and in the asymptotic region. In Fig. 5, we show the potential energy curve created by varying the bond angle with the bond length set to 0.9578 Å. In the region analyzed with $r = 2$, the XBK method is unable to find energies lower than the RHF method, while the QCC method demonstrates a marked improvement in accuracy at every bond angle.
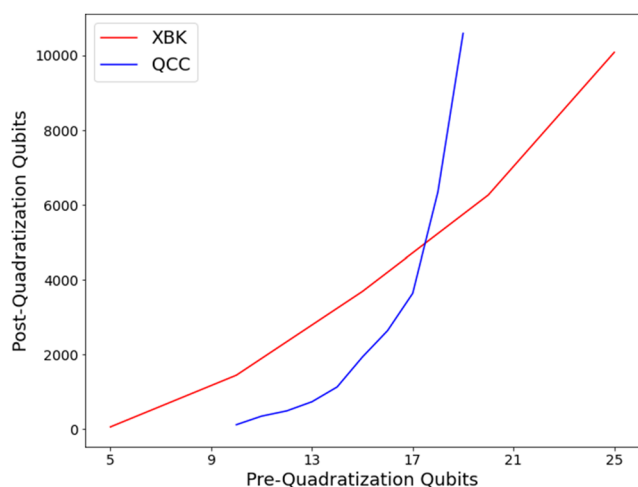
FIG. 6. Number of post-quadratization qubits required to run each method vs the number of pre-quadratization qubits for H_2O with a bond length of 1.6 Å.

FIG. 7. Breakdown of the computation times of the XBK and QCC methods vs the number of pre-quadratization qubits for H_2O with a bond length of 1.6 Å.

The calculated values of the binding energy, bond length, and bond angle of H_2O are shown in Table II. Since the XBK method returned the RHF energies near the equilibrium point, the calculated bond length and angle are the same as in the RHF method. The binding energy is closer to that given by the CASCI method due to the asymptotic behavior of the XBK method. The QCC method nears the chemical accuracy for the binding energy and shows improvement for the bond length and angle.

Figures 6 and 7 show the qubit and time scaling, respectively, of H_2O with a bond length of 1.6 Å. For H_2O, the number of pre-quadratization qubits is $5r$ for the XBK method and $10 + N_{ent}$ for the QCC method. Figure 6 thus indicates that the number of post-quadratization qubits required to simulate H_2O surpasses what is available on the Advantage system after $r = 3$ and $N_{ent} = 7$. The scaling of both metrics is similar to the results for H_3^+, indicating that as the number of pre-quadratization qubits increases, the resource requirements increase rapidly. The CASCI method required just 0.38 s.

VI. CONCLUDING REMARKS

As demonstrated in Secs. II–V, it is possible to perform electronic structure calculations by using quantum annealers in tandem with a classical computer. However, we see that the time required to run the XBK and QCC methods is much greater than their classical counterparts. The reasons for this are twofold: first, the requirement that the problem Hamiltonian mapped on the annealer be two-local results in an exponential increase in the number of qubits as ancillary qubits are introduced during quadratization, necessitating more qubits on the annealer and leading to longer run times, and second, each method requires extensive time-consuming use of the classical computer, erasing any potential quantum speedup.

The XBK method requires a large number of pre-quadratization qubits to achieve results much better than the RHF method. Since the number of post-quadratization qubits increases rapidly with the number of pre-quadratization qubits, the XBK method thus quickly surpasses the number of qubits available on modern annealers, making the accurate simulation of larger molecules difficult. The QCC method demonstrates improvement over the XBK method by achieving a greater level accuracy using fewer qubits. Unfortunately, the QCC method leans on the classical computer more heavily by using it to perform the bulk of the optimization. Hence, the computation time of the QCC method scales largely the same as the classical optimization algorithm used. In addition, the number of post-quadratization qubits increases even faster for the QCC method such that using the method for systems much larger than H_2O is only possible with very few entanglers and minimal folding, resulting in very little improvement over the RHF energies. For these reasons, neither method is able to accurately simulate all but the smallest of molecules.

There are a few potential avenues through which the speed and accuracy of quantum chemical simulations on quantum annealers can be improved. From the software side, new methods could be developed to map the problem Hamiltonian to the Ising model using fewer qubits. This could involve either a more efficient transformation to z-type Pauli operators or better techniques for utilizing molecular symmetries. A potential hardware solution, which would likely be much more beneficial, would be to develop large-scale annealers implementing non-stoquastic Hamiltonians.[12–14,16,17] Such an annealer would be universal and could utilize methods such as Hamiltonian gadgets to quadratize the Hamiltonian.[33,34] This would enable one to avoid the introduction of large numbers of ancillary qubits during the quadratization process and to more efficiently simulate larger molecules.

ACKNOWLEDGMENTS

DATA AVAILABILITY

The data that support the findings of this study are available from the corresponding author upon reasonable request.

REFERENCES

[1] J. D. Whitfield, J. Biamonte, and A. Aspuru-Guzik, "Simulation of electronic structure Hamiltonians using quantum computers," Mol. Phys. **109**, 735–750 (2011).

[2] A. Peruzzo, J. R. McClean, P. Shadbolt, M.-H. Yung, X. Zhou, P. J. Love, A. Aspuru-Guzik, and J. L. O'Brien, "A variational eigenvalue solver on a photonic quantum processor," Nat. Commun. **5**, 4213 (2014).

[3] R. Xia and S. Kais, "Quantum machine learning for electronic structure calculations," Nat. Commun. **9**, 4195 (2018).

[4] K. Choo, A. Mezzacapo, and G. Carleo, "Fermionic neural-network states for *ab initio* electronic structure," Nat. Commun. **11**, 2368 (2020).

[5] R. Xia, T. Bian, and S. Kais, "Electronic structure calculations and the Ising Hamiltonian," J. Phys. Chem. B **122**, 3384–3395 (2018).

[6] S. N. Genin, I. G. Ryabinkin, and A. F. Izmaylov, "Quantum chemistry on quantum annealers," arXiv:1901.04715 [physics.chem-ph] (2019).

[7] T. Kadowaki and H. Nishimori, "Quantum annealing in the transverse Ising model," Phys. Rev. E **58**, 5355–5363 (1998).

[8] A. Das and B. K. Chakrabarti, "Colloquium: Quantum annealing and analog quantum computation," Rev. Mod. Phys. **80**, 1061–1081 (2008).

[9] D. de Falco and D. Tamascelli, "An introduction to quantum annealing," RAIRO: Theor. Inf. Appl. **45**, 99–116 (2011).

[10] A. Ambainis and O. Regev, "An elementary proof of the quantum adiabatic theorem," arXiv:0411152v2 [quant-ph] (2006).

[11] M. Amin, "Searching for quantum speedup in quasistatic quantum annealers," Phys. Rev. A **92**, 052323 (2015).

[12] J. Biamonte and P. Love, "Realizable Hamiltonians for universal adiabatic quantum computers," Phys. Rev. A **78**, 012352 (2008).

[13] W. Vinci and D. A. Lidar, "Non-stoquastic Hamiltonians in quantum annealing via geometric phases," npj Quantum Inf. **3**, 38 (2017).

[14] E. K. Grant and T. S. Humble, "Adiabatic quantum computing and quantum annealing," in *Oxford Research Encyclopedia* (2020).

[15] A. Cho, "Quantum or not, controversial computer yields no speedup," Science **344**, 1330–1331 (2014).

[16] R. Barends, A. Shabani, L. Lamata, J. Kelly, A. Mezzacapo, U. L. Heras, R. Babbush, A. G. Fowler, B. Campbell, Y. Chen, Z. Chen, B. Chiaro, A. Dunsworth, E. Jeffrey, E. Lucero, A. Megrant, J. Y. Mutus, M. Neeley, C. Neill, P. J. J. O'Malley, C. Quintana, P. Roushan, D. Sank, A. Vainsencher, J. Wenner, T. C. White, E. Solano, H. Neven, and J. M. Martinis, "Digitized adiabatic quantum computing with a superconducting circuit," Nature **534**, 222–226 (2016).

[17] I. Ozfidan, C. Deng, A. Y. Smirnov, T. Lanting, R. Harris, L. Swenson, J. Whittaker, F. Altomare, M. Babcock, C. Baron, A. Berkley, K. Boothby, H. Christiani, P. Bunyk, C. Enderud, B. Evert, M. Hager, A. Hajda, J. Hilton, S. Huang, E. Hoskinson, M. Johnson, K. Jooya, E. Ladizinsky, N. Ladizinsky, R. Li, A. MacDonald, D. Marsden, G. Marsden, T. Medina, R. Molavi, R. Neufeld, M. Nissen, M. Norouzpour, T. Oh, I. Pavlov, I. Perminov, G. Poulin-Lamarre, M. Reis, T. Prescott, C. Rich, Y. Sato, G. Sterling, N. Tsai, M. Volkmann, W. Wilkinson, J. Yao, and M. H. Amin, "Demonstration of a nonstoquastic Hamiltonian in coupled superconducting flux qubits," Phys. Rev. Appl. **13**, 034037 (2020).

[18] I. G. Ryabinkin, S. N. Genin, and A. F. Izmaylov, "Constrained variational quantum eigensolver: Quantum computer search engine in the Fock space," J. Chem. Theory Comput. **15**, 249–255 (2019).

[19] S. Bravyi and A. Y. Kitaev, "Fermionic quantum computation," Ann. Phys. **298**, 210–226 (2002).

[20] J. T. Seeley, M. Richard, and P. J. Love, "The Bravyi-Kitaev transformation for quantum computation of electronic structure," J. Chem. Phys. **137**, 224109 (2012).

[21] A. Tranter, S. E. Sofia, J. Seeley, M. Kaicher, J. R. McClean, R. Babbush, P. V. Coveney, F. Mintert, F. K. Wilhelm, and P. J. Love, "The Bravyi-Kitaev transformation: Properties and applications," Int. J. Quantum Chem. **115**, 1431–1441 (2015).

[22] S. Bravyi, J. M. Gambetta, A. Mezzacapo, and K. Temme, "Tapering off qubits to simulate fermionic Hamiltonians," arXiv:1701.08213 [quant-ph] (2017).

[23] K. Setia, R. Chen, J. E. Rice, A. Mezzacapo, M. Pistoia, and J. Whitfield, "Reducing qubit requirements for quantum simulation using molecular point group symmetries," J. Chem. Theory Comput. **16**, 6091–6097 (2020).

[24] M. Anthony, E. Boros, Y. Crama, and A. Gruber, "Quadratic reformulations of nonlinear binary optimization problems," Math. Program. **162**, 115–144 (2017).

[25] N. Dattani, "Quadratization in discrete optimization and quantum mechanics," arXiv:1901.04405 [quant-ph] (2019).

[26] I. G. Ryabinkin, T.-C. Yen, S. N. Genin, and A. F. Izmaylov, "Qubit coupled cluster method: A systematic approach to quantum chemistry on a quantum computer," J. Chem. Theory Comput. **14**, 6317–6326 (2018).

[27]P. Atkins and R. Friedman, *Molecular Quantum Mechanics*, 5th ed. (Oxford University Press, 2011).

[28]Q. Sun, T. C. Berkelbach, N. S. Blunt, G. H. Booth, S. Guo, Z. Li, J. Liu, J. McClain, E. R. Sayfutyarova, S. Sharma, S. Wouters, and G. K.-L. Chan, "PySCF: The python-based simulations of chemistry framework," Wiley Interdiscip. Rev.: Comput. Mol. Sci. **8**, e1340 (2018).

[29]J. R. McClean, K. J. Sung, I. D. Kivlichan, Y. Cao, C. Dai, E. S. Fried, C. Gidney, B. Gimby, P. Gokhale, T. Häner, T. Hardikar, V. Havlíček, O. Higgott, C. Huang, J. Izaac, Z. Jiang, X. Liu, S. McArdle, M. Neeley, T. O'Brien, B. O'Gorman, I. Ozfidan, M. D. Radin, J. Romero, N. Rubin, N. P. D. Sawaya, K. Setia, S. Sim, D. S. Steiger, M. Steudtner, Q. Sun, W. Sun, D. Wang, F. Zhang, and R. Babbush, "OpenFermion: The electronic structure package for quantum computers," arXiv:1710.07629 [quant-ph] (2017).

[30]D-Wave Ocean Software, D-Wave Systems.

[31]V. Choi, "Minor-embedding in adiabatic quantum computation: I. The parameter setting problem," Quantum Inf. Process. **7**, 193–209 (2008).

[32]R. Byrd, P. Lu, J. Nocedal, and C. Zhu, "A limited memory algorithm for bound constrained optimization," SIAM J. Sci. Comput. **16**, 1190–1208 (1995).

[33]R. Babbush, P. J. Love, and A. Aspuru-Guzik, "Adiabatic quantum simulation of quantum chemistry," Sci. Rep. **4**, 6603 (2015).

[34]Y. Cao, R. Babbush, J. Biamonte, and S. Kais, "Hamiltonian gadgets with reduced resource requirements," Phys. Rev. A **91**, 012315 (2015).

[35]M. Streif, F. Neukart, and M. Leib, "Solving quantum chemistry problems with a D-wave quantum annealer," arXiv:1811.05256 [quant-ph] (2019).